Examining long-term variability in saturated hydraulic conductivity of sandy soils and its influencing factors

Saeed Nikghalb Ashouri[1], Adrian Pittari[1] , Vicki Moon[1], Ali Shokri[1]

1. Waikato University, New Zealand

Abstract

Saturated hydraulic conductivity (*Ks*) is a crucial parameter that influences water flow in saturated soils, with applications in various fields such as surface water runoff, soil erosion, drainage, and solute transport. However, accurate estimation of *Ks* is challenging due to temporal and spatial uncertainties. This study addresses the knowledge gap regarding the long-term behaviour of *Ks* in sandy soils with less than 10% fine particles. The research investigates the changes in *Ks* over a long period of constant head tests and examines the factors influencing its variation. Two sandy samples were tested using a hydraulic conductivity cell, and the hydraulic head and discharge were recorded for over 50 days. The results show a general decline in *Ks* throughout the test, except for brief periods of increase. Furthermore, the relationship between flow rate and hydraulic head gradient does not follow the expected linear correlation from Darcy's law, highlighting the complex nature of sandy soil hydraulic conductivity. The investigation of soil properties in three different sections of the samples before and after the tests revealed a decrease in the percentage of fine particles and a shift in specific gravity from the bottom to the top of the sample, suggesting particle migration along the flow direction. Factors such as clogging by fine particles and pore pressure variation contribute to the changes in *Ks*. The implications of this study have far-reaching effects on various geotechnical engineering applications. These include groundwater remediation, geotechnical stability analysis, and drainage system design.

Keywords: Saturated hydraulic conductivity, constant head test, clogging, sandy soil, drainable pores

1. Introduction

The saturated hydraulic conductivity (*Ks*) plays a crucial role in determining the water flow rate within the saturated zone of soils. This parameter is essential in various fields of study, including surface water runoff, soil erosion, deep percolation, drainage, crop simulation models, and solute transport (Ben-Hur et al., 2009; Boadu, 2000; Hwang et al., 2017; Suleiman & Ritchie, 2001). Using

the Darcy equation, *Ks* can be defined as the ratio of water flow (*Q*) in the unit section of saturated soil (*A*) to the hydraulic gradient (*i*). The parameter *Ks* is present in the majority of equations related to water flow in a saturated medium, yet its estimation can be challenging both in the laboratory and the field due to temporal and spatial uncertainties (Suleiman & Ritchie, 2001).

Laboratory estimations of *Ks* utilise three standard methods: constant head, falling head, and constant flow rate, as detailed in ASTM D5856-15 (2015). When dealing with granular and disturbed samples containing less than 10% of fine particles passing 75 μm or No. 200 sieve, the recommended approach is the constant head method, as outlined in ASTM D2434-19 (2019). Conversely, samples comprising more than 10% of fine particles can be analysed using any of the three mentioned methods. However, *Ks* measurements are conducted using a rigid-wall, compaction-mold permeameter, with specific criteria provided in ASTM D5856 (2015).

Extensive research has been conducted on the long-term variations of hydraulic conductivity in low-permeability soils, which are commonly employed in landfill sites and artificial wetlands. From the perspective of an Earth scientist, these materials might be perceived as loose sediment or deposits rather than the conventional 'soil,' which typically encompasses a mixture of inorganic and organic constituents. In landfills, leachate, and artificial wetlands, contaminated water from roads needs to be contained to gradually remove the pollutants from the water and prevent pollution of underground water resources (Fang et al., 2022; Li et al., 2023; Shaver, 2020; Touze-Foltz et al., 2006; Valencia-González et al., 2022; W. Wang et al., 2023). Therefore, the application of a layer with very low permeability is necessary to reduce the infiltration of contaminated water into the soil while simultaneously eliminating pollutants. Several studies have shown that the *Ks* in low permeability soil samples change with infiltration of the water that contains chemical or biological agents (Francisca & Glatstein, 2010; Liu & Liu, 2020; Lu et al., 2020; Montoro & Francisca, 2010).

Chemical substances present in the fluid can create a chemical imbalance and interfere with ion exchange processes in the soil, leading to fluctuations in *Ks*. According to a study conducted by Jo et al. (2005), a 3-year test observed a tenfold variation in *Ks* of a clay liner permeated by leachate-containing chemical agents. In their tests, the hydraulic conductivity of one of the samples reached stability after about 1.5 years of the test. On the other hand, the formation of microorganisms and the presence of nutrients to feed them can cause clogging in the soil and, hence, a reduction in the drainable pores and *Ks* (Fang et al., 2022; VanGulck & Rowe, 2004).

In sandy soils, the duration of the test is usually relatively short. It is commonly assumed that the test can be concluded when four samples yield values within ±25% of the mean calculated from

these four samples throughout the test (ASTM D5856-15, 2015). Also, there is no reference to the length of the test in ASTM D2434-19 (2019). However, several studies suggest that the hydraulic conductivity of sandy soils can change over time. For example, there has been extensive research on the variation of hydraulic conductivity in groundwater artificial recharge (Konikow et al., 2001; Mays & Hunt, 2005; Siriwardene et al., 2007; Song et al., 2020; Ye et al., 2019). Vanderzalm et al. (2020) and Du et al. (2018) subjected sandy samples to water permeation containing suspended solids and *Fe (III)* ions, respectively, for an extended period (40 days in the former case and seven days in the latter study), leading to observed fluctuations in *Ks* that demonstrate a prevalent declining pattern over time. These studies identified physical and biological clogging mechanisms as dominant factors for *Ks* variation. However, neither of the above studies has tested a sample permeated with distilled water or tap water with minimum suspended solids or chemicals to ensure that *Ks* remains constant under minimum influent contamination. Du et al. (2013) and Z. Wang Et al. (2012) used tap water with and without suspended solids in a constant head test on quartz sand samples and observed a noticeable drop in *Ks* over four days. Siriwardene et al. (2007) also reported a reduction in the *Ks* when the sample was permeated with tap water containing suspended solids. They noticed clogging of the suspended solids in the lower section of the sample as the main reason for the noticeable drop in the *Ks*, whereas Z. Wang et al. (2012) showed that finer suspended solids could travel deeper in the sample and cause blockage of the drainable pores.

Clogging can also be caused by the internal mobilisation or swelling of fine particles in the soil (Jeong et al., 2018a; Konikow et al., 2001; Mohan et al., 1993; Torkzaban et al., 2015). Additionally, clay minerals like *Illite*, *Kaolinite*, and *Montmorillonite* can be washed with water, leading to the blockage of drainable pores in the sample and a reduction in *Ks* (Cihan et al., 2022; Jeong et al., 2018a; Y. Wang et al., 2021). Stormwater management devices like artificial soakage basins and soak pits are commonly recommended in new urban developments with high infiltration rates (Shaver, 2020). Furthermore, with the widespread use of artificial groundwater recharge, the long-term behaviour of *Ks* in sandy materials gains significant importance. Variations in *Ks* and pore blockages can profoundly influence the effectiveness of design strategies employed in stormwater management and groundwater recharge scenarios.

Currently, there is a lack of research focusing on the extended-duration variations in *Ks* within sandy soils due to fluctuating hydraulic levels. Observing *Ks* over the long term provides insights into the sustained groundwater movement within the aquifer, with changes in hydraulic levels indicating shifts in aquifer water levels during and after rainfall events. This study aims to bridge the knowledge gap regarding the prolonged behaviour of hydraulic conductivity in sandy soils.

Although various research has explored short-term *Ks* variations, particularly in the context of stormwater management devices, a comprehensive understanding of how *Ks* evolves over extended timeframes remains limited. Grasping the long-term behaviour of *Ks* holds critical significance for the effectiveness of soakage systems and safeguarding subsurface water resources. Thus, this paper illuminates the key factors shaping *Ks* variations over prolonged periods.

2. Materials

2.1. Sample source and physical properties

The soil examined in this study is river sand, commercially referred to as pit sand, often employed for embankments and raised areas like pathways. The pit sand used for this investigation originated from sand quarries situated in Ngahinapouri and Te Kowhai, located along the Waipa River in Waikato, New Zealand, as depicted in Figure 1. For this study, two samples (sample *A* and sample *B*) were taken from the same batch of pit sand provided by a supplier. Sample *B* was used as a replication in this research.

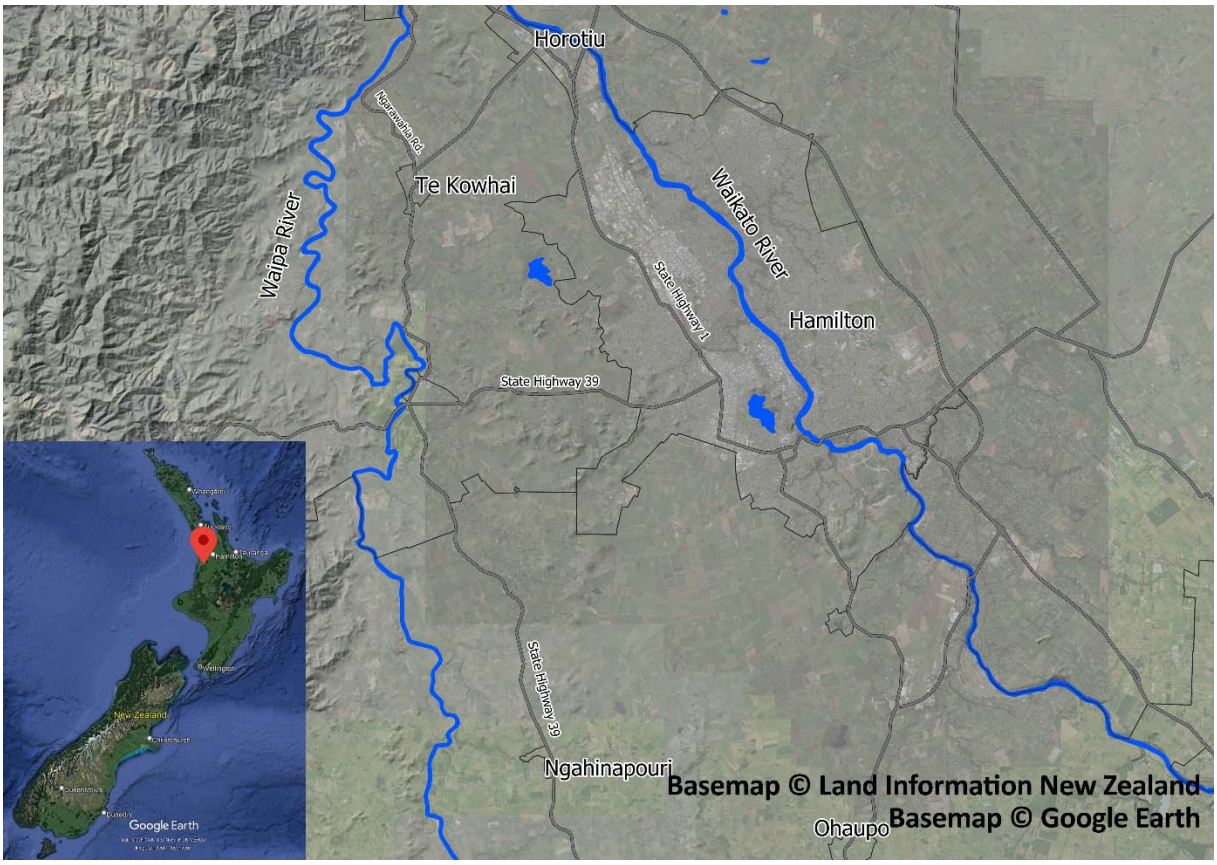

Figure 1- The geographical location of the Waipa River in New Zealand, with the samples originating from sand quarries located near the Waipa riverbanks.

Table 1 outlines the physical properties of the samples. Upon microscopic examination and particle separation, five distinct groups are discerned (Figure 2): quartz and feldspar (approximately 60%), pumice (approximately 11%), colourful particles (approximately 6%), magnetics (approximately 10%), and glass shards (approximately 13%). The magnetic minerals were isolated through magnetic separation. X-ray diffraction (XRD) analysis was employed to assess mineral composition, while the loss on ignition (LOI) method was utilised to estimate the presence of organic material in the samples. The analysis of XRD data peak patterns confirms that quartz and feldspar constitute the majority of minerals in the sample (Figure 3).

A laser diffractometer (Malvern Mastersizer 3000) was used to determine the particle size distribution of the samples. For this study, the particles below 75 *μm* were considered as fines, which aligns with the classification of ASTM for fine and coarse particles (ASTM D2487, 2020). The particle size distribution results indicate that the samples are primarily sandy, with less than 10% of fine materials. Particles below 5 *μm* were considered mobile colloidal particles (Kretzschmar et al., 1999), and the percentages of these particles are also mentioned in Table 1. Based on Standard Proctor tests (ASTM, 2012), the optimal compaction moisture of the samples was determined to be 12%.

Table 1- Properties of tested samples

Parameter	Sample A	Sample B
Specific gravity of grains	2.6739	-
Specific surface (m^2/kg)	84.60	102.90
Particles < 5 μm (%)	2.3	2.6
Particles 5-75 μm (%)	5.06	5.83
Particles > 75 μm (%)	92.61	91.56
Dry density (g/cm^3)	1.289	1.261
Optimal gravimetric compaction moisture (%)	12	12
Sample gravimetric moisture (%)*	8.1	11.8
Organic matter	1.7%	1.7%

* Sample gravimetric moisture was measured when the sample was compacted in the mould. A small amount of sample A and B was taken and dried in the oven, and moisture was measured.

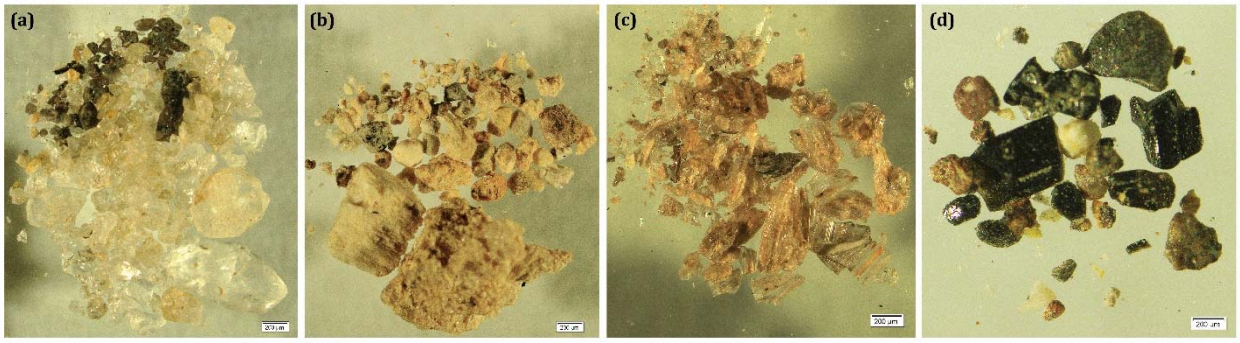

Figure 2- Separation of particles under microscope: (a) Quartz and feldspar, (b) Pumice, (c), glass shards, and (d) colourful minerals

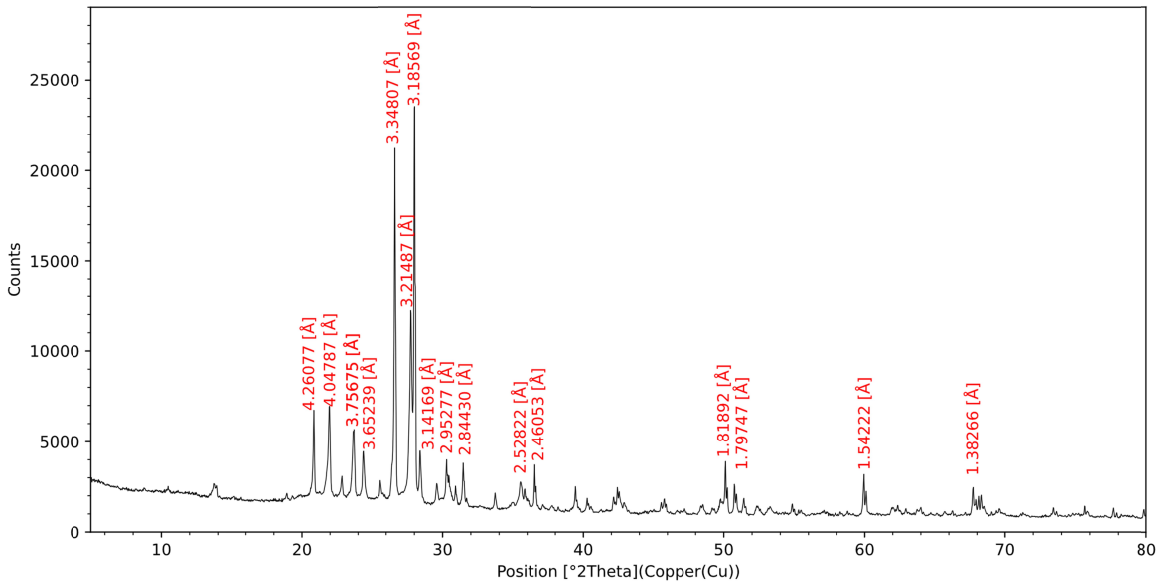

Figure 3- XRD analysis of the sample: Major peaks are related to the quartz and feldspar content in the sample

2.2. Sample preparation

Prior to conducting the tests, the samples underwent a preparation process that involved drying in an oven at 105℃ for 24 hours and passing through a 2 *mm* sieve. The moist tamping method was used to prepare the samples, which is based on a technique described by Ladd (1978). This method allows for achieving a uniform distribution of density in the sample. A specific amount of soil was weighed, and distilled water was sprayed onto the samples to attain an initial moisture content of 8.1% (Sample A) and 11.8% (Sample B). The choice of 8.1% moisture for sample A was intended to explore the influence of initial compaction moisture on the extended-term variations of *Ks*. The samples were then covered and left for approximately 24 hours to achieve moisture balance before

testing. The samples were compacted in a constant head test cell with an interior diameter and height of 76.2 *mm* and 292 *mm*, respectively. Compaction was carried out in layers of 12 *mm*. Before the compaction, subsamples were taken to measure the actual moisture, particle size distribution, and XRD. The final dry density of the samples was calculated from the net dry soil used and compacted sample volume and listed in The soil examined in this study is river sand, commercially referred to as pit sand, often employed for embankments and raised areas like pathways. The pit sand used for this investigation originated from sand quarries situated in Ngahinapouri and Te Kowhai, located along the Waipa River in Waikato, New Zealand, as depicted in Figure 1. For this study, two samples (sample *A* and sample *B*) were taken from the same batch of pit sand provided by a supplier. Sample *B* was used as a replication in this research.

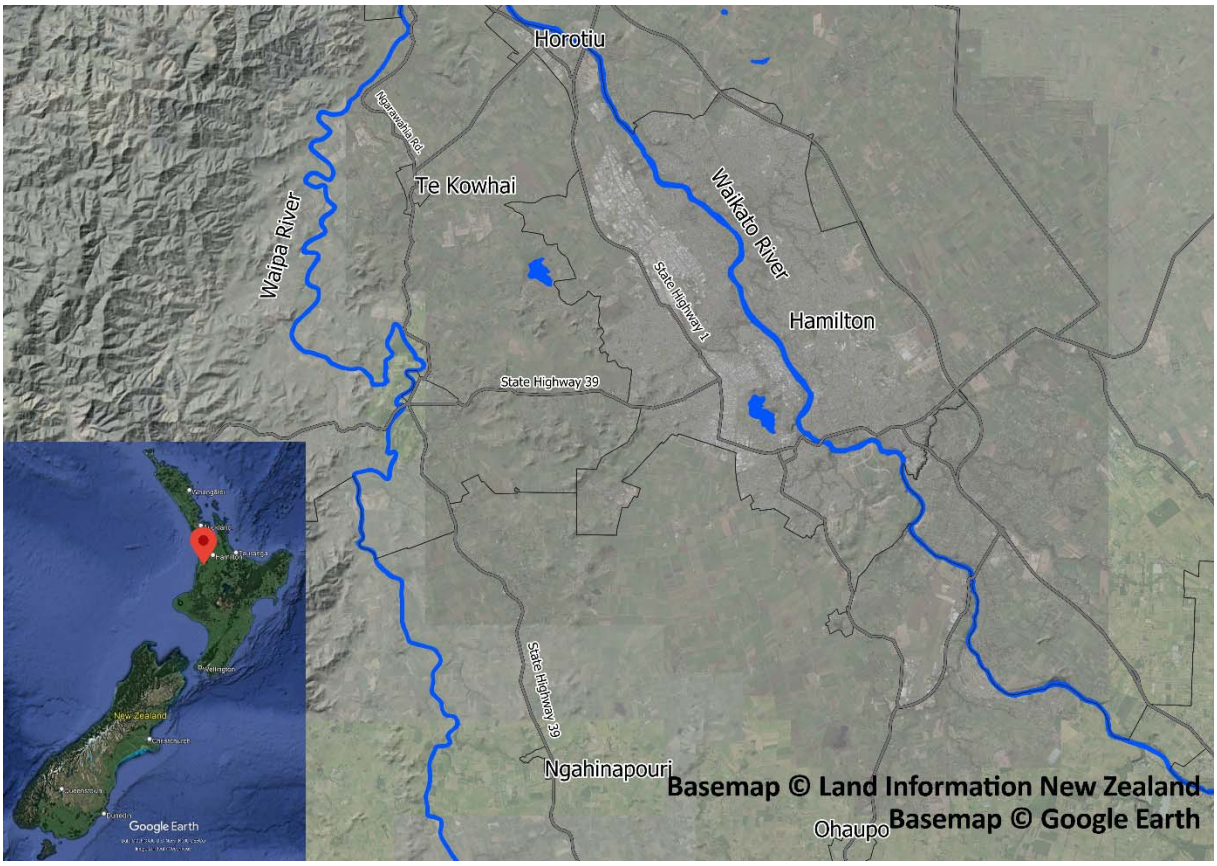

Figure 1- The geographical location of the Waipa River in New Zealand, with the samples originating from sand quarries located near the Waipa riverbanks.

Table 1 outlines the physical properties of the samples. Upon microscopic examination and particle separation, five distinct groups are discerned (Figure 2): quartz and feldspar (approximately 60%), pumice (approximately 11%), colourful particles (approximately 6%), magnetics (approximately 10%), and glass shards (approximately 13%). The magnetic minerals were isolated through

magnetic separation. X-ray diffraction (XRD) analysis was employed to assess mineral composition, while the loss on ignition (LOI) method was utilised to estimate the presence of organic material in the samples. The analysis of XRD data peak patterns confirms that quartz and feldspar constitute the majority of minerals in the sample (Figure 3).

A laser diffractometer (Malvern Mastersizer 3000) was used to determine the particle size distribution of the samples. For this study, the particles below 75 μm were considered as fines, which aligns with the classification of ASTM for fine and coarse particles (ASTM D2487, 2020). The particle size distribution results indicate that the samples are primarily sandy, with less than 10% of fine materials. Particles below 5 μm were considered mobile colloidal particles (Kretzschmar et al., 1999), and the percentages of these particles are also mentioned in Table 1. Based on Standard Proctor tests (ASTM, 2012), the optimal compaction moisture of the samples was determined to be 12%.

Table 1.

To achieve saturation, the samples were first connected to a vacuum pump for one hour. Distilled and de-aired water was then introduced into the test cell in an upward direction, following the procedure outlined in ASTM D2434-19 (ASTM, 2019), to minimise air entrapment. The samples were left saturated overnight to reduce the chances of air entrapment further.

3. Methods

3.1. Constant head hydraulic conductivity tests

The schematic experimental apparatus used for the constant head hydraulic conductivity test is shown in Figure 4. The adjustable water head tank enabled the alteration of the hydraulic head during the experiment without the need to terminate the test. In addition, there were porous disks with a 1 *mm* mesh size and a spring on top to hold the sample stable in the cell. The mesh size of the porous disk was selected in a way to prevent the formation of clogging and pressure drops on the disk.

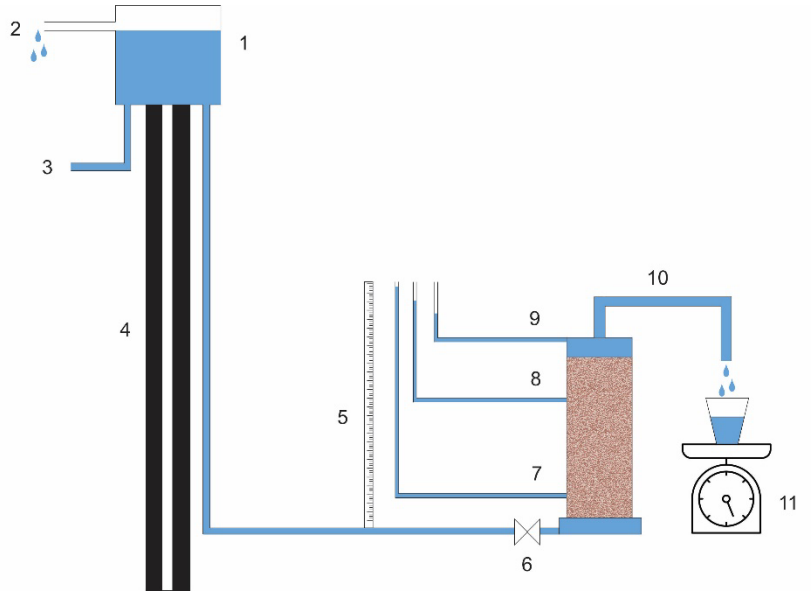

Figure 4-Schematic constant head hydraulic conductivity apparatus-(1) Water tank, (2) overflow outlet, (3) water supply hose, (4) adjustable level board, (5) ruler, (6) water entrance valve, (7) piezometer 1, (8) piezometer 2, (9) piezometer 3, (10) water outlet, (11) scale for measuring the discharge

The water flow and head gradient were measured at least thrice daily. The collection of effluent in a bucket was carried out for each flow measurement, and the duration of the effluent collection was recorded. Subsequently, the discharge was calculated by dividing the weight of the collected effluent by the collection duration.

The tests were conducted in a back-and-forth pattern with water heads ranging from 963 *mm* to 1765 *mm*, with increments and decrements of approximately 200 *mm*. The hydraulic head began at a minimum of 963 *mm* and was incrementally increased by around 200 *mm* until it reached a maximum of 1765 *mm*. Subsequently, the head followed the same pattern of decrease in sequential steps. The testing period has lasted for approximately 53 days. Detailed information on the test numbers, hydraulic heads, and durations can be found in **Error! Reference source not found.**.

Table 2- Hydraulic Head and Durations of Constant Head Tests on Samples A and B

Test Number	**1**	**2**	**3**	**4**	**5**	**6**	**7**	**8**	**9**	**10**
Hydraulic head (mm)	963	1163	1365	1558	1765	1558	1365	1163	963	Varies
Sample A Duration (days)	5	6	6	6	5	3	7	6	7	1

Sample B Duration (days)	5	5	5	5	5	5	5	5	31	N/A

During the testing process, the pressure and discharge readings were recorded simultaneously by three piezometers. As depicted in Figure 4, the pressure inside the sample was measured by two piezometers located at points 7 and 8, while the piezometer at point 9 measured the water head at the discharge point on the opposite end of the cell.

After completing test 9 on sample *A*, the water flow was not stopped, and a moderately rapid constant head test was conducted using the same hydraulic heads as tests 1 to 9. This test, designated as "Test 10", lasted approximately 16 hours, with each constant head being run for about 2 hours. The purpose of Test 10 was to observe any changes in *Ks* under a shorter duration and to determine if the *Ks* during the head-increasing stage were similar to the reciprocal *Ks* during the head-decreasing stage.

In the case of sample *B*, test 9 was allowed to run for 31 days at the minimum head (963 *mm*) after an increasing trend in the *Ks* of the sample was observed from day 53 onwards. The purpose was to determine how long the *Ks* would continue to change and whether it would return to a value similar to the beginning of the test.

In order to examine changes in soil properties during the test, the samples were recovered from the hydraulic conductivity cell. After extraction, the samples were divided into three sections: bottom, middle, and top. Subsequently, particle size distribution and specific gravity measurements were conducted on these sub-samples to assess any variations resulting from the test.

4. Results

4.1. Long-term *Ks* Tests

The long-term change in *Ks* calculated for both samples is illustrated in Figure 5. The *Ks* values of the samples showed a general decline throughout the tests, as shown in Figure 5, except for three brief periods. These periods occurred between days 36 to 38 for sample *A* and between days 0 to 1 and 37 to 40 for sample *B*.

Furthermore, there are two distinct periods of a noticeable increase in *Ks* in both samples, which coincide closely in timing, specifically between days 35 and 40. In sample *A*, the increase in *Ks* starts at 1365 *mm* head and ends at the same head in Figure 5a. However, in sample *B*, *Ks* starts

increasing at 1163 *mm* head and starts decreasing again at 963 *mm* head in Figure 5b. There is no clear answer to why *Ks* increases in the mentioned periods in the samples. At the end of the tests, the final *Ks* values for samples *A* and *B* were 96% and 91% lower than their maximum, respectively.

The initial moisture levels (8.1% for sample A and 11.8% for sample B) appear to have had limited influence on the extended-term variation of *Ks*. However, they might have played a role in the initial stages of permeation. Figure 5 illustrates that sample *A* achieved its maximum *Ks* within the first few hours of commencing the test. In contrast, sample *B* took approximately two days to reach its peak *Ks*.

Also, throughout the head increase cycle, a notable pattern emerges: at the onset of each hydraulic head increment, there is a marginal uptick in *Ks*, which is subsequently followed by a sustained decrease. This minor elevation in *Ks* can be attributed to the abrupt rise in the hydraulic head.

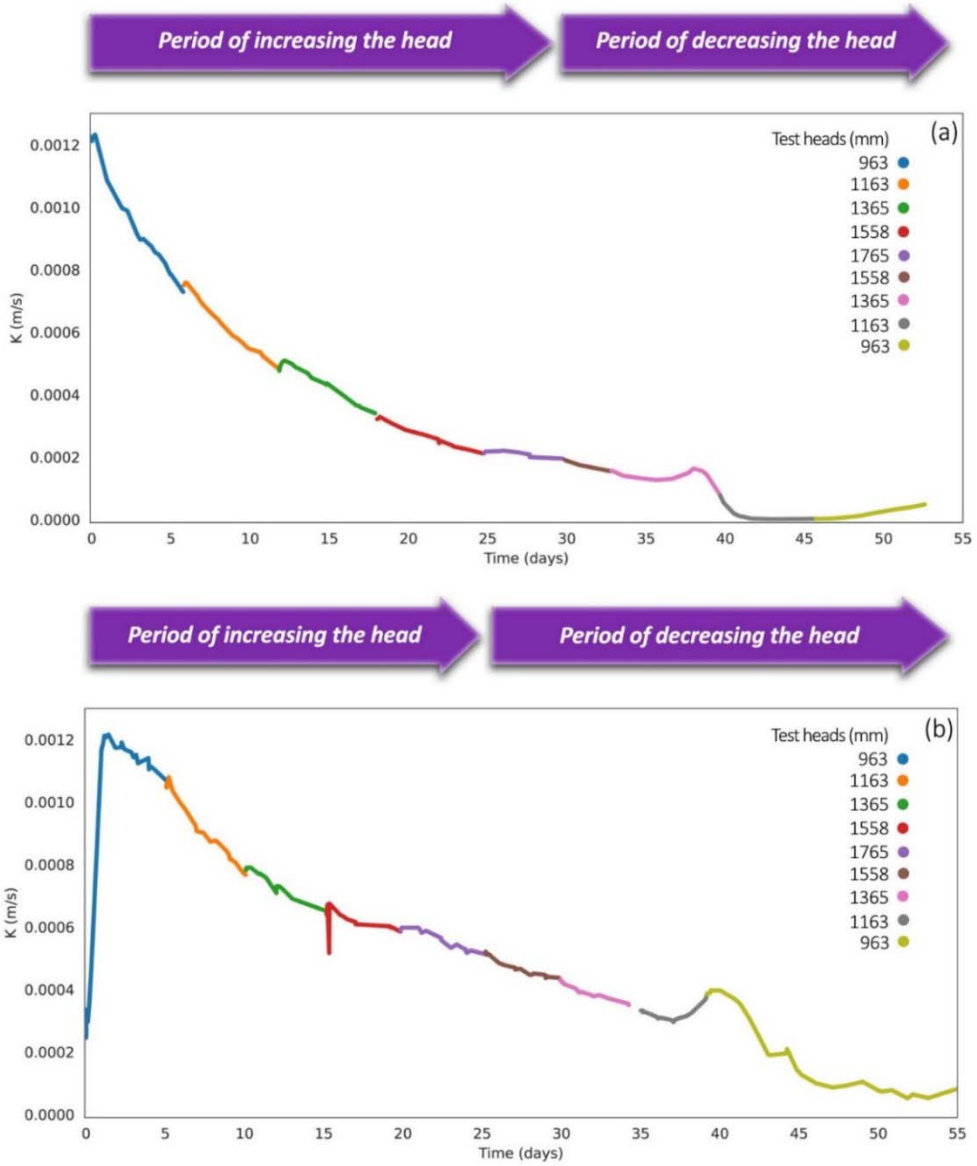

Figure 5- Changes of Ks over time for samples A (a) & B (b)- the generally reducing trend in Ks is noticeable in both samples

4.2. Flow-head gradient relationship

In the hypothetical scenario, where the samples remained unchanged throughout the tests, Darcy's law would anticipate the clustering of all data points at each hydraulic head increment around a single point, forming a unified line. Figure 6 illustrates the relationship between flow rate (Q) and hydraulic head gradient (i) within samples A and B across varying hydraulic head levels. The symbol "R" signifies the period characterised by a decreasing head. The scatterplots demonstrate the absence of a straightforward linear correlation between Q and i.

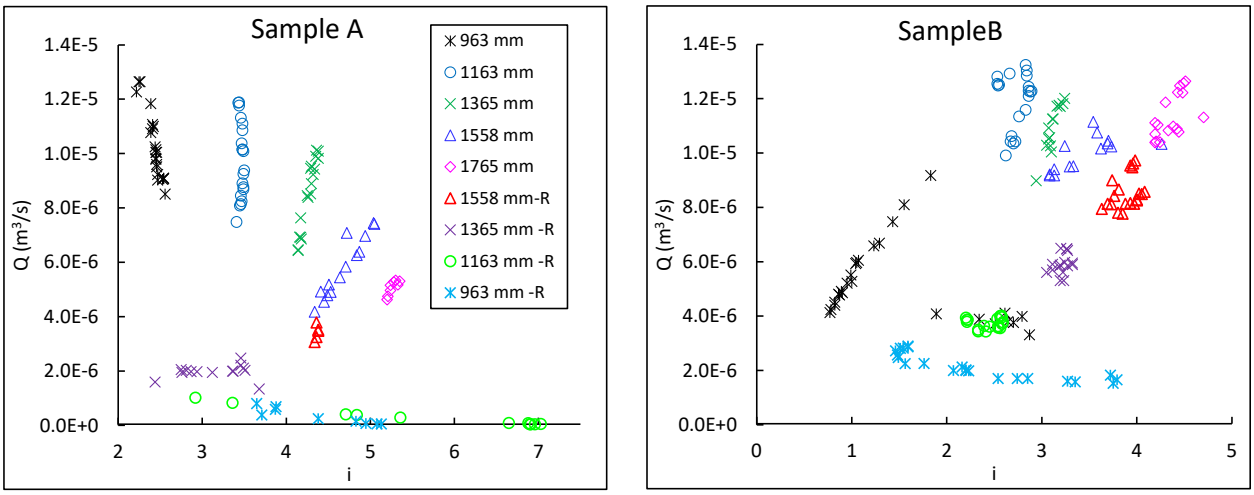

Figure 6: Scatterplots exploring the correlation between head gradient and flow rate in samples A and B with different hydraulic head levels. The symbol "R" signifies the period characterised by a decreasing hydraulic head.

In the case of sample A, during test phases 1 to 4, wherein the head is incrementally raised every 5 or 6 days from 963 to 1765 mm, a decrease in flow accompanied by an increase in head gradient becomes evident. Interestingly, even within each step, the scatterplot does not exhibit the expected convergence around a single point, as outlined by Darcy's law. This suggests a dynamic nature of the sample during this period, with the hydraulic conductivity undergoing continuous changes. However, test 5, characterised by the maximum head of 1765 mm and a 5-day observation period, showcases a remarkable consistency in both head gradient and flow rate, implying a phase of stability.

Furthermore, as the head is reduced to 1558mm, this stability persists, with the scatterplot points clustering around a single location and both flow rate and head gradient diminishing. On the contrary, during tests 7 to 9, where the head drops from 1365 to 963 mm, the scatterplot points display unpredictable distribution, deviating significantly from the expectations of Darcy's law. This observation indicates a departure from the anticipated behaviour of the sample.

In sample B, the initial test with a head of 963 mm shows an unexpected trend where both the head gradient and flow rate increase, deviating from the expected convergence around a single point. As we move through tests 2 to 4, involving a hydraulic head increase from 1163 to 1558 mm, a distinct behaviour emerges: despite the elevated hydraulic head, the head gradient rises while the flow rate unexpectedly drops. This pattern suggests a shift in the hydraulic properties of the samples.

Nevertheless, when the hydraulic head is raised to 1765 mm and subsequently reduced to 1163 mm over four 5-day intervals, the sample aligns somewhat better with the predictions of Darcy's law. Data points cluster more closely around a central location, and the flow rate responds to changes in the hydraulic head. However, variations still exist at each step. In contrast, at the lowest head level of 963 mm, there's an increase in head gradient while the flow rate remains stable.

4.3. Sample A behaviour in a relatively short-duration test

Test 10 was carried out to ensure that the variations in *Ks* and *Q-i* relation are not noticeable in the short term. In this test, the sample exhibited a distinct behaviour compared to the other tests. The test involved subjecting the sample to a cycle of increasing and decreasing hydraulic heads, similar to the previous tests, but for a shorter period of approximately 16 hours.

Interestingly, this relatively quick test demonstrated a strong linear correlation between the water flux and the gradient within the sample, as expected by the Darcy law. The hydraulic conductivity was determined to be 7×10^{-7} *m/s* during the increasing stage of the test head and 8×10^{-7} *m/s* during the decreasing stage. The correlation between *Q* and *i* is illustrated in Figure 7. Contrary to Figure 6, a notably stronger correlation between *Q* and *i* can be observed.

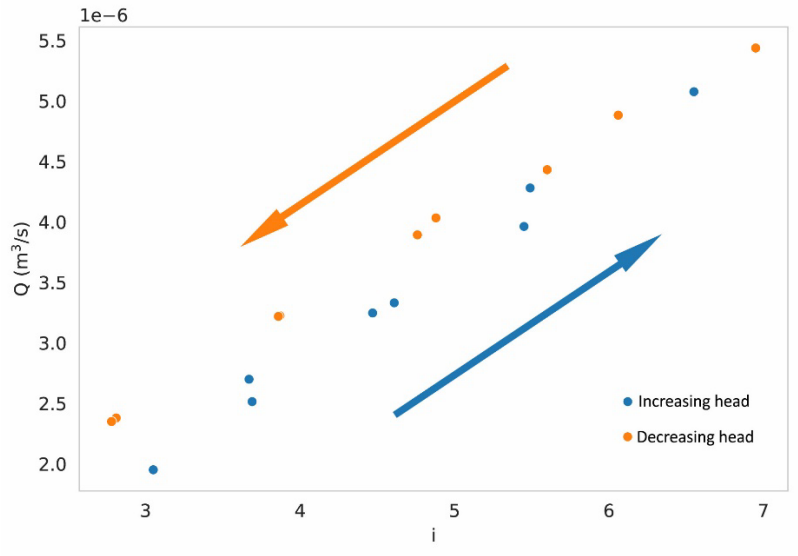

Figure 7- The relationship between Q and i in test 10 for sample A, where the gradients are varied. The blue and orange arrows represent the periods of increasing and decreasing test heads, respectively.

4.4. Extending the sample B in the minimum constant head for 31 days

Test B has been extended for an additional 31-day period under the minimum head condition (963 mm). This extension aims to investigate whether hydraulic conductivity comes into stability without any disruptions.

Figure 8(a) depicts the correlation between flow rate and head gradient during this period. The *Q-i* correlation exhibits unpredictable fluctuations in both hydraulic gradient and flow rate, mirroring the patterns observed in the preceding 45 days, as shown in Figure 6.

The temporal evolution of *Ks* is visually outlined in Figure 8(b). The variability of *Ks* spans from 1.25×10^{-4} m/s to 0.5×10^{-4} m/s, centring around a median value of 1.0×10-4 mm. In summary, the continuation of the testing procedure with a consistent hydraulic head maintained over the course of 31 days does not result in the stabilisation of the hydraulic conductivity of the sample. The *Ks* values persistently oscillate within a range of +33% and -46% around the median value, thereby underscoring the absence of stability in the system. However, a decreasing trend is absent in contrast to previous observation periods.

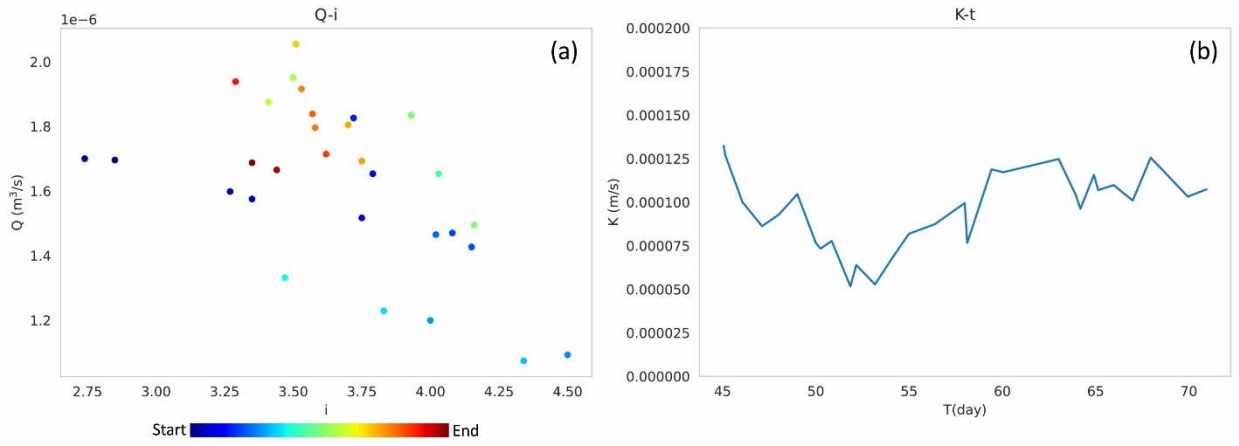

Figure 8- (a) The relationship between Q and i for sample B during an extended period (31 days) of running test 9 at the minimum hydraulic head. The colour spectrum and arrows depict the temporal sequence of the measurements. (b) The changes in Ks over time for sample B during the same 31-day duration of test 9 at the minimum hydraulic head.

4.5. Comparison of soil properties before and after the tests

In order to assess the influence of the constant head test on soil properties, particle size distribution (PSD) and specific gravity (GS) measurements were performed on both the original soil samples and different sections of the soil after the test. This investigation aimed to understand how the test influenced the PSD and density characteristics of the soil samples.

Figure 9 shows the *PSD* of the sample's top, middle, and bottom sections and the original sample prior to the test. Additionally, Table 3 compares the total particles below and above 75 μm for reference. The results in Table 3 indicate that the sample's total percentage of fine particles decreased after the tests. Approximately 2% of fine particles in sample *A* and 1% in sample *B* were washed away during the long-term tests. It is noteworthy that samples *A* and *B* contained less than 9% of fine particles (below 75 μm).

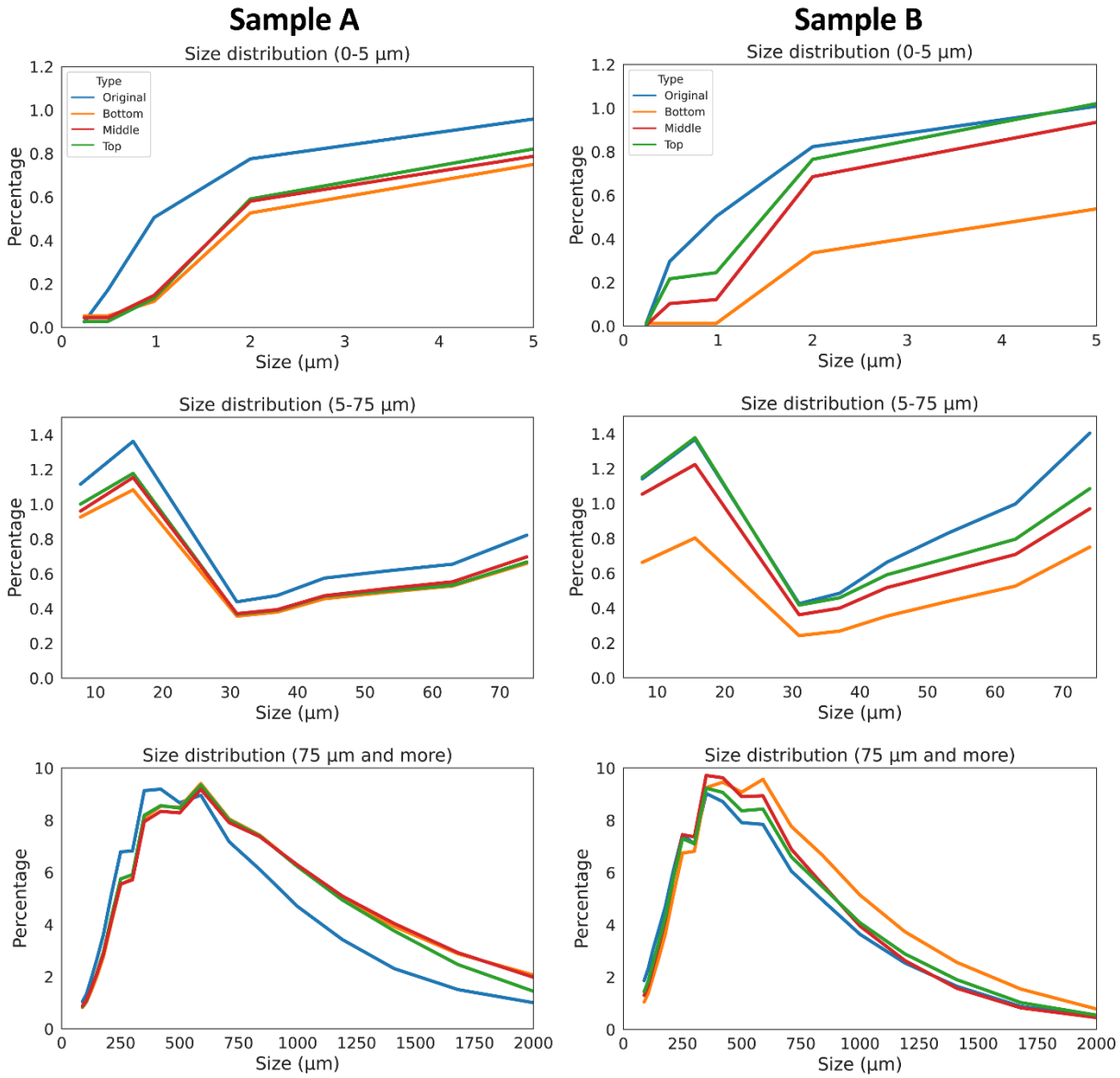

Figure 9- Particle size analysis of the samples (comparison of the samples before tests and after tests, divided by sub-samples of different sections)

Table 3- Comparison of total percentage of particles below and above 64 µm before and after tests divided by different sections in the sample

	Sample A				Sample B			
Totals (%)	Original	Bottom	Middle	Top	Original	Bottom	Middle	Top
Below 75 µm	7.37	5.09	5.41	5.74	8.42	4.06	6.68	7.63
Above 75 µm	92.61	94.91	94.59	94.26	91.58	95.94	93.32	92.37

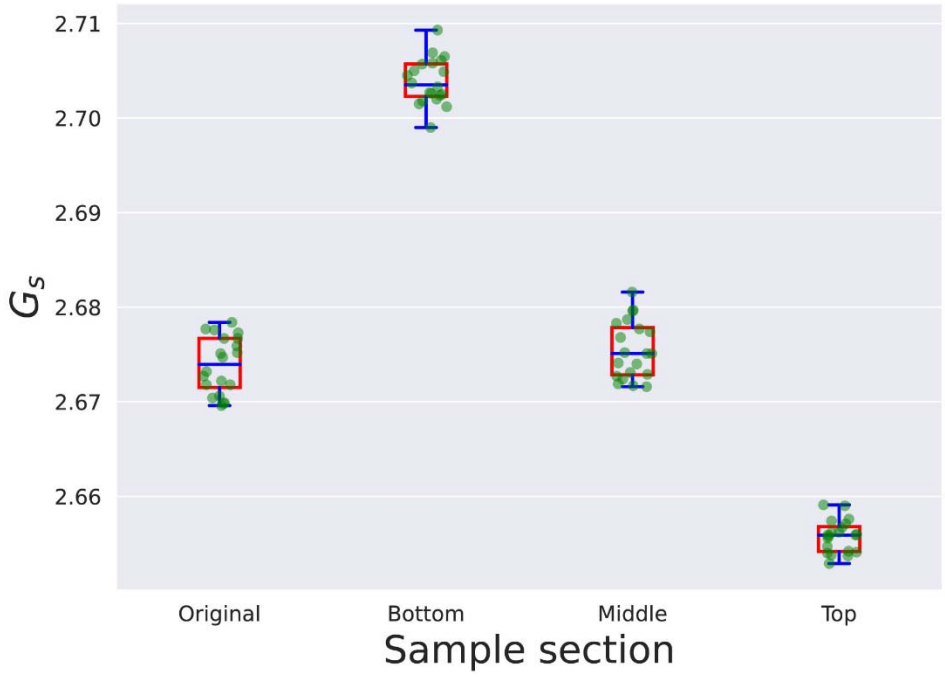

Figure 10- Specific gravity of sample A before and after test divided by sub-samples of different sections

Figure 9 and Table 3 show that the percentage of fine particles below 75 µm is highest at the top section of the samples, followed by the middle and bottom sections. While the difference in the percentage of fine particles among different sections is minor for sample A (less than 1%), it is higher for sample B (around 3%).

Gs measurements are presented as a box plot in Figure 10. The box plots illustrate notable changes in the specific gravity of the sample in comparison to the original sample. The lowest *Gs* is found at

337 the bottom section of sample A, while the highest *Gs* is observed at the top section, with a slight
338 increase in the middle section.

339 5. Discussion

340 Examining soil properties in the original sample before and after the constant head test reveals
341 notable alterations in the soil characteristics. These changes directly impact the hydraulic
342 conductivity, highlighting the direct influence of the test on soil properties and subsequent
343 hydraulic behaviour. For example, Figure 5(a & b) demonstrates a prevailing long-term decreasing
344 trend in *Ks*. However, it is important to note that there are also intermittent shorter periods where
345 *Ks* show an increase. This observation highlights the dynamic nature of the system, wherein both
346 long-term trends and shorter-term fluctuations in hydraulic conductivity are evident.

347 The *Ks* tests on the coarse particles (sandy samples with less than 10% fines) are generally short
348 because the variation of *Ks* is very marginal during the first few hours of the tests. For example, in
349 sample *A*, the change of *Ks* during the first 5 hours from starting the test was only 2%, which is
350 negligible. However, after five days, the *Ks* dropped by 40%, and at the end of the test, the *Ks*
351 dropped by around 96% from the beginning of the test.

352 Figure 6 clearly represents the dynamic nature of the samples' hydraulic gradient and pore
353 pressure. These parameters undergo continuous fluctuations without exhibiting a consistent
354 decreasing or increasing pattern. Even extending the test for a longer period (Figure 8 (a) and (b))
355 does not create a stable gradient in the sample. Therefore, it can be inferred that the connectivity of
356 the drainable pores is constantly changing. This observation underscores the complex behaviour of
357 the hydraulic system within the samples, emphasising the need to consider the temporal variations
358 in pore pressure when analysing the overall hydraulic response.

359 The variations in the hydraulic gradient and discharge relation, and hence hydraulic conductivity in
360 the samples, can be attributed to several factors. According to the ASTM standard (ASTM, 2015), air
361 entrapment can potentially reduce hydraulic conductivity. In this research, a primary focus was
362 minimising air entrapment within the sample during saturation. As a result, no visible evidence of
363 air entrapment was observed during the test. The transparent acrylic test cell facilitated direct
364 observation of the sample particles throughout the experiment. The absence of any noticeable
365 formation of air bubbles among the particles from the sides of the samples suggests that air
366 entrapment is unlikely to contribute to the observed reduction in *Ks* in our study.

Another factor that can affect the continuous reduction of *Ks* is the blockage of drainable pores with fine particles (Jeong et al., 2018b), which restricts the flow of water and leads to a decrease in the *Ks*. Particle size distribution of the samples (Figure 9) shows that the fine particles in all sections have decreased compared to the original sample prior to the test. Furthermore, there is a decrease in *Gs* in the top section and an increase in the bottom section (Figure 10). It can be concluded that mobile low-density fine particles (such as fine pumice) have displaced from the bottom of the sample to the top. Another reason for the reduction in the *Ks* can be related to the continuous blockage of the drainable pores with fine particles with rough surfaces (such as glass shards) or the simultaneous impact of blockage by glass shards and mobilisation and blockage by low-density particles. The SEM image of the sample in Figure 11 shows a noticeable amount of glass shards and pumice in the small section of the sample. Continuous mobilisation or re-deposition of these particles can change the connection of the drainable pores and reduce *Ks*.

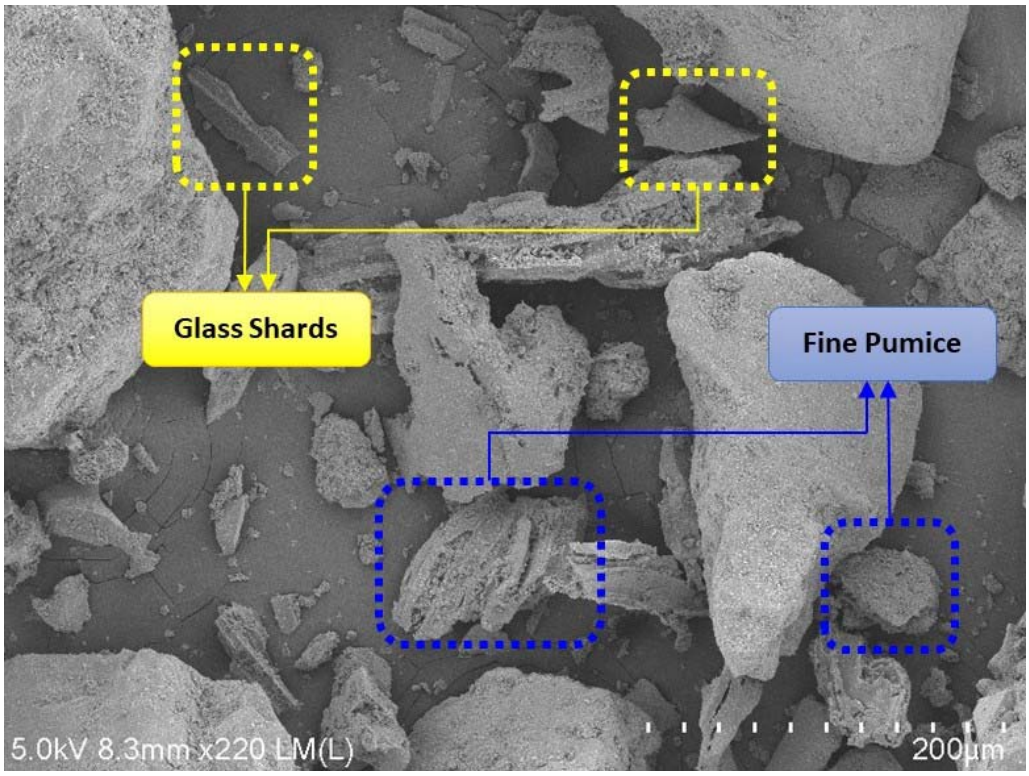

Figure 11- 220x magnification of the sample using SEM providing a closer view of the fine particles in the sample

The ASTM standard for granular soils (ASTM, 2019a) explains the procedure of estimating the *Ks* without mentioning the period of carrying out each test. The long-term *Ks* results in Figure 6 show a noticeable drop in the *Ks*, and if the test is terminated in a few hours, the resulting *Ks* will be 96%

higher than the final one. Similar results were reported by (Du et al., 2018; Vanderzalm et al., 2020), when they permeated the sample with a solution containing *Fe (III)* or water with suspended solids. In our research, there was no *Fe (III)* contamination source, and the water used was drinking water from a tap. Figure 7 demonstrates a robust linear relationship between *Q* and *i* during the increasing and decreasing head phases during short-term testing. However, when comparing this figure to the long-term tests illustrated in Figure 6, it becomes evident that the *Q-i* relationship varies over time.

The long-term variability of hydraulic conductivity holds significant importance for systems enduring extended saturation periods. For instance, artificial soakage basins and soak pits are frequently recommended in the context of stormwater management in new urban developments (Shaver, 2020). These systems gather runoff from urban areas and gradually infiltrate the water into the ground. A crucial factor in designing these soakage systems is the saturated hydraulic conductivity. However, it's important to note that the testing duration commonly used to assess the *Ks* rate is often short and may not accurately represent the long-term behaviour of hydraulic conductivity. Consequently, it's wise to account for the long-term variation of Ks when reporting *Ks* values for applications involving soil saturation, such as soakage basins or drainage pipes. This precaution is essential as overestimation could lead to erroneous calculations.

6. Conclusion

This study provides valuable insights into the variation of hydraulic conductivity in sandy samples through a long-term constant head experiment. The results demonstrate a significant reduction in *Ks*, primarily due to physical clogging caused by fines and pumice particles. The increased concentration of pumice particles in the top section indicates their mobility and potential blockage of drainable pore sections, affecting *Ks*. These changes were not observed in short-term tests, highlighting the importance of longer-term investigations. The findings stress the need for extended constant head tests to accurately assess and report *Ks* in sandy samples, enhancing our understanding of their hydraulic behaviour. These findings have practical implications in various geotechnical engineering applications, such as groundwater remediation, landfill design, geotechnical stability analysis, and drainage system design.

7. Acknowledgment

This research was supported by the University of Waikato Doctoral Scholarship.

8. Data Availability Statement

All data used and generated by this study, including hydraulic head and flow measurements, can be found in PDI-36052.

9. References

ASTM. (2019). Standard Test Method for Permeability of Granular Soils (Constant Head) (D2434-19). *ASTM International, West Conshohocken, PA*. https://doi.org/10.1520/D2434-19

ASTM D2434-19. (2019). Standard Test Method for Permeability of Granular Soils (Constant Head). *ASTM International, West Conshohocken, PA*. https://doi.org/10.1520/D2434-19

ASTM D2487. (2020). Standard Practice for Classification of Soils for Engineering Purposes (Unified Soil Classification System). *ASTM*.

ASTM D5856-15. (2015). Standard Test Method for Measurement of Hydraulic Conductivity of Porous Material Using a Rigid-Wall, Compaction-Mold Permeameter. *ASTM International, West Conshohocken, PA*.

Ben-Hur, M., Yolcu, G., Uysal, H., Lado, M., & Paz, A. (2009). Soil structure changes: Aggregate size and soil texture effects on hydraulic conductivity under different saline and sodic conditions. *Australian Journal of Soil Research*. https://doi.org/10.1071/SR09009

Boadu, F. K. (2000). Hydraulic Conductivity of Soils from Grain-Size Distribution: New Models. *Journal of Geotechnical and Geoenvironmental Engineering*, *126*(8), 739–746. https://doi.org/10.1061/(ASCE)1090-0241(2000)126:8(739)

Chaneva, J., Kluger, M. O., Moon, V. G., Lowe, D. J., & Orense, R. P. (2023). Monotonic and cyclic undrained behaviour and liquefaction resistance of pumiceous, non-plastic sandy silt. *Soil Dynamics and Earthquake Engineering*, *168*, 107825. https://doi.org/10.1016/j.soildyn.2023.107825

Cihan, A., Petrusak, R., Bhuvankar, P., Alumbaugh, D., Trautz, R., & Birkholzer, J. T. (2022). Permeability Decline by Clay Fines Migration around a Low-Salinity Fluid Injection Well. *Groundwater*, *60*(1), 87–98. https://doi.org/10.1111/gwat.13127

Du, X., Wang, Z., & Ye, X. (2013). Potential Clogging and Dissolution Effects During Artificial Recharge of Groundwater Using Potable Water. *Water Resources Management*, *27*(10), 3573–3583. https://doi.org/10.1007/S11269-013-0365-5/FIGURES/13

Du, X., Zhang, H., Ye, X., & Lu, Y. (2018). Flow Velocity Effects on Fe(III) Clogging during Managed Aquifer Recharge Using Urban Storm Water. *Water 2018, Vol. 10, Page 358*, *10*(4), 358. https://doi.org/10.3390/W10040358

Fang, Y., Kong, L., Zhang, P., Zhang, L., Zhao, H., Xiang, X., Cheng, S., Zhang, H., Ju, F., & Li, L. (2022). Fifteen-year analysis of constructed wetland clogging: A critical review. *Journal of Cleaner Production*, *365*, 132755. https://doi.org/https://doi.org/10.1016/j.jclepro.2022.132755

Francisca, F. M., & Glatstein, D. A. (2010). Long term hydraulic conductivity of compacted soils permeated with landfill leachate. *Applied Clay Science*. https://doi.org/10.1016/j.clay.2010.05.003

Hwang, H. T., Jeen, S. W., Suleiman, A. A., & Lee, K. K. (2017). Comparison of saturated hydraulic conductivity estimated by three different methods. *Water (Switzerland)*. https://doi.org/10.3390/w9120942

Jeong, H. Y., Jun, S. C., Cheon, J. Y., & Park, M. (2018a). A review on clogging mechanisms and managements in aquifer storage and recovery (ASR) applications. *Geosciences Journal*, *22*(4), 667–679. https://doi.org/10.1007/S12303-017-0073-X/METRICS

Jeong, H. Y., Jun, S.-C., Cheon, J.-Y., & Park, M. (2018b). A review on clogging mechanisms and managements in aquifer storage and recovery (ASR) applications. *Geosciences Journal*, *22*(4), 667–679. https://doi.org/10.1007/s12303-017-0073-x

Jo, H. Y., Benson, C. H., Shackelford, C. D., Lee, J.-M., & Edil, T. B. (2005). Long-Term Hydraulic Conductivity of a Geosynthetic Clay Liner Permeated with Inorganic Salt Solutions. *Journal of Geotechnical and Geoenvironmental Engineering*. https://doi.org/10.1061/(asce)1090-0241(2005)131:4(405)

Kikkawa, N., Orense, R. P., & Pender, M. J. (2013). Observations on microstructure of pumice particles using computed tomography. *Canadian Geotechnical Journal*, *50*(11), 1109–1117. https://doi.org/10.1139/cgj-2012-0365

Konikow, L. F., August, L. L., & Voss, C. I. (2001). Effects of Clay Dispersion on Aquifer Storage and Recovery in Coastal Aquifers. *Transport in Porous Media*, *43*(1), 45–64. https://doi.org/10.1023/A:1010613525547

Kretzschmar, R., Borkovec, M., Grolimund, D., & Elimelech, M. (1999). *Mobile Subsurface Colloids and Their Role in Contaminant Transport* (pp. 121–193). https://doi.org/10.1016/S0065-2113(08)60427-7

Ladd, R. (1978). Preparing Test Specimens Using Undercompaction. *Geotechnical Testing Journal*, *1*(1), 16. https://doi.org/10.1520/GTJ10364J

Li, K., Chen, Y., Ye, W., & Wang, Q. (2023). Modelling the evolution of dual-pore structure for compacted clays along hydro-mechanical paths. *Computers and Geotechnics*, *157*, 105308. https://doi.org/https://doi.org/10.1016/j.compgeo.2023.105308

Liu, L., Orense, R., & Pender, M. (2015). Crushing-induced liquefaction characteristics of pumice sand. *Proc., Australia-New Zealand Conference on Geomechanics*.

Liu, Y., & Liu, J. (2020). The BioChemical Clogging of Landfill Leachate Collection System: Based on Laboratory Studies. *International Journal of Environmental Research and Public Health*, *17*(7), 2299. https://doi.org/10.3390/ijerph17072299

Lu, H., Wang, C., Li, D., Li, J., & Wan, Y. (2020). Permeability, Pore, and Structural Parameters of Undisturbed Silty Clay Presented in Landfill Leachate. *Water, Air, & Soil Pollution*, *231*(5), 190. https://doi.org/10.1007/s11270-020-04568-0

Mays, D. C., & Hunt, J. R. (2005). Hydrodynamic Aspects of Particle Clogging in Porous Media. *Environmental Science & Technology*, *39*(2), 577–584. https://doi.org/10.1021/es049367k

Mohan, K. K., Vaidya, R. N., Reed, M. G., & Fogler, H. S. (1993). Water sensitivity of sandstones containing swelling and non-swelling clays. *Colloids and Surfaces A: Physicochemical and Engineering Aspects*, *73*, 237–254. https://doi.org/10.1016/0927-7757(93)80019-B

Montoro, M. A., & Francisca, F. M. (2010). Soil Permeability Controlled by Particle-Fluid Interaction. *Geotechnical and Geological Engineering*. https://doi.org/10.1007/s10706-010-9348-y

Shaver, E. (2020). Waikato stormwater management guideline.

Siriwardene, N., Deletic, A., & Fletcher, T. (2007). Clogging of stormwater gravel infiltration systems and filters: Insights from a laboratory study. *Water Research*, *41*(7), 1433–1440. https://doi.org/10.1016/j.watres.2006.12.040

Song, W., Liu, X., Zheng, T., & Yang, J. (2020). A review of recharge and clogging in sandstone aquifer. *Geothermics*, *87*, 101857. https://doi.org/10.1016/j.geothermics.2020.101857

Suleiman, A. A., & Ritchie, J. T. (2001). Estimating saturated hydraulic conductivity from soil porosity. *Transactions of the American Society of Agricultural Engineers*. https://doi.org/10.13031/2013.4683

Torkzaban, S., Bradford, S. A., Vanderzalm, J. L., Patterson, B. M., Harris, B., & Prommer, H. (2015). Colloid release and clogging in porous media: Effects of solution ionic strength and flow velocity. *Journal of Contaminant Hydrology*, *181*, 161–171. https://doi.org/10.1016/j.jconhyd.2015.06.005

Touze-Foltz, N., Duquennoi, C., & Gaget, E. (2006). Hydraulic and mechanical behavior of GCLs in contact with leachate as part of a composite liner. *Geotextiles and Geomembranes*, *24*(3), 188–197. https://doi.org/https://doi.org/10.1016/j.geotexmem.2006.01.004

Valencia-González, Y., Quintero-Ramírez, A., & Lara-Valencia, L. A. (2022). A laboratory methodology for predicting variations in the geotechnical parameters of soil exposed to solid waste leachates in the field. *Results in Engineering*, *14*, 100398. https://doi.org/https://doi.org/10.1016/j.rineng.2022.100398

Vanderzalm, J. L., Page, D. W., Barry, K. E., & Gonzalez, D. (2020). Evaluating Treatment Requirements for Recycled Water to Manage Well Clogging during Aquifer Storage and Recovery: A Case Study in the Werribee Formation, Australia. *Water 2020, Vol. 12, Page 2575*, *12*(9), 2575. https://doi.org/10.3390/W12092575

VanGulck, J. F., & Rowe, R. K. (2004). Evolution of clog formation with time in columns permeated with synthetic landfill leachate. *Journal of Contaminant Hydrology*. https://doi.org/10.1016/j.jconhyd.2004.06.001

Wang, W., Dong, L., Zhai, T., Wang, W., Wu, H., Kong, F., Cui, Y., & Wang, S. (2023). Bio-clogging mitigation in constructed wetland using microbial fuel cells with novel hybrid air-photocathode. *Science of The Total Environment*, *881*, 163423. https://doi.org/https://doi.org/10.1016/j.scitotenv.2023.163423

Wang, Y., Yu, M., Bo, Z., Bedrikovetsky, P., & Le-Hussain, F. (2021). Effect of temperature on mineral reactions and fines migration during low-salinity water injection into Berea

sandstone. *Journal of Petroleum Science and Engineering*, *202*, 108482. https://doi.org/10.1016/j.petrol.2021.108482

Wang, Z., Du, X., Yang, Y., & Ye, X. (2012). Surface clogging process modeling of suspended solids during urban stormwater aquifer recharge. *Journal of Environmental Sciences*, *24*(8), 1418–1424. https://doi.org/10.1016/S1001-0742(11)60961-3

Ye, X., Cui, R., Du, X., Ma, S., Zhao, J., Lu, Y., & Wan, Y. (2019). Mechanism of Suspended Kaolinite Particle Clogging in Porous Media During Managed Aquifer Recharge. *Groundwater*, *57*(5), 764–771. https://doi.org/10.1111/gwat.12872